CHAPTER SIX

Shapes and Surface Characteristics

Shapes and Sizes

Since the great majority of iron meteorites are finds (see page 37), it might be feared that their ablational sculpture is greatly modified by terrestrial corrosion. An attempt has been made in this study to assert the importance of corrosion. In Appendix 1, the last column indicates whether the heat-affected α_2 zone, page 51, and the fusion crust are preserved. If this is the case, one may confidently assume that less than 2 mm of the exterior has on the average been lost by weathering. That is, the meteorites display in all major features their external shape as it was immediately after the fall. An analysis of the data shows that of 480 iron meteorites, 146 display both fusion crust and α_2 zone, while 230 display only α_2 zones. In other words roughly half of the known irons are only insignificantly corroded, and their shapes may be taken as a true representation of the form they had immediately after landing.

Inspection of these some 200 iron meteorites gives the impression of an almost endless variety of shapes. See Table 22.

Further details and some photographs of the shapes and sizes will be found in the individual descriptions. Only a few generalizations will be attempted here.

Our main interest in the shape and size of the meteorites is perhaps due to our curiosity about their *preatmospheric* shape and size. These data are absolutely unknown and can, at the moment, only be attained by judicious evaluation of the surviving masses. For cosmic ray studies, it is imperative to know the degree of shielding; i.e., to know how much iron was superimposed upon the present meteorite in space but was ablated away in the atmosphere. For the same reason it is also necessary to know whether an analyzed sample comes from a primary or a secondary, i.e., a fragmentation surface from atmospheric flight.

Since we know that a significant thickness (1-4 mm/sec) is ablated away in flight, it is best to examine large iron meteorites which have lost proportionately least mass first. Bacubirito and Mbosi display tabular, flattened shapes which apparently are a true representation of their cosmic shape. Campo del Cielo, Cape York, Tucson and Chupaderos were probably also tabular originally but burst in the atmosphere to produce more or less angular fragments.

Another shape which must be quite common in space is the angular, pyramidal shape, perhaps bounded by mineral-rich fracture surfaces of octahedral, dodecahedral and hexahedral orientations. Some of these oriented faces have survived ablation surprisingly well in, e.g., Quesa, Repeev Khutor, Calico Rock and Edmonton (Canada). In the latter two, adjacent cubic faces are barely rounded.

With more effective ablation (higher velocity and longer trajectories) the original angular shapes are severely altered. If the meteorite acquires a stabilized flight, an original pyramidal apex may assume the shape of a more or less perfect cone, as is the case for Morito, Willamette, Tamentit, Zerhamra, Grant, Oakley and Quinn Canyon. This, of course, requires that the meteorite was oriented at entry with the pyramidal apex in the flight direction. Morito, Grant and numerous others display prominent flight markings that support the supposition of oriented flight. The regmaglypts on the skirt of the cone are elongated and radiate away from the apex. Along the edge between the cone and the rear side spilled-over ablation melts may be observed. The flat rear sides are only slightly ablated and probably represent the best known approximations to preatmospheric surfaces.

Cones may also be carved from angular fragments *that were produced in flight*. It is thus remarkable that beautiful low cones are known from the shower- and crater-producing meteorites, Sikhote-Alin, Wabar and Henbury. The cone-shaped Sikhote-Alin masses were obviously produced by early fragmentation and long independent flights of perhaps 30 km.

The cone-shaped masses from Wabar and Henbury require special attention, since the bulk of these meteorites were lost by cratering impact. The cones cannot just be bombshell fragments from the explosion; these, which may also be found at the impact site, are entirely different in appearance. The cones must be near-surface parts on the original body that separated high in the atmosphere, continued in independent flight and thus escaped the cratering shock waves. The material is, therefore, of great value as complimentary to the bombshells which were altered during impact. For similar reasons it is believed that the meteorites around other prominent craters, such as Canyon Diablo, Odessa and Boxhole, may be divided into two categories, one which had independent flights and suffered little shock alterations and one which represents shock-altered surviving explosion fragments.

Some of the more curious shapes have undoubtedly been produced by bursting in the atmosphere. This is true of the "icicles" of Glorieta Mountain and the "crossed fingers" of Sikhote-Alin, which represent fragments separated along phosphide-filled octahedral grain boundaries. The small masses of the Mundrabilla shower obtained their remarkable shapes by splitting along troilite-filled austenite grain boundaries and subsequent ablation. It is likely that the ring shape of Tucson was produced when a large flattened fragment separated along the flow-lines of oriented silicate inclusions across which the coherence was low. Kokstad-Matatiele form another ring which, however, broke late in flight. The jaw-like Hex River and Mount Magnet masses are probably remnants of rings, the remaining parts of which were never found.

If the falling meteorite keeps tumbling, it will probably ultimately acquire angular-equixial shapes and, if the trajectory is long, perhaps occasionally approach the ovoid or spherical shape.

Ellipsoidal shapes with numerous variations are more common, however. Among these the huge zeppelin-shaped Babb's Mill (Blake's Iron) is remarkable and difficult to understand. Discoid masses and ovoid masses are quite common, but generally small, below 15 kg. The seven smallest iron meteorites (see Table 21) are ovoid or lenticular and quite smooth, with only occasional regma-

Table 22. Shapes of Well-preserved Iron Meteorites

Approximate shape	Examples
Airfoil	Costilla Peak, Jamestown, Nelson County, Sacramento Mountains, Seneca Township, Wood's Mountain
Shield or very low cones	Cabin Creek, Davis Mountains, Ilimaes, Iron Creek, N'Goureyma, Murnpeowie, Oakley, Roebourne, Sikhote-Alin (1745 kg), Tamentit
Low cones	Chebankol, Henbury, Hraschina, Quinn Canyon, Reed City, Uegit, Wabar, Zerhamra
High cones	Freda, Grant, Linville, Morito, Repeev Khutor, Serrania de Varas, Surprise Springs, Willamette, Withrow
Spheroidal, or with spheroidal parts	Bogou, Briggsdale, Durango, Hassi-Jekna, Keen Mountain, Mount Ouray, Muzzaffarpur, Roebourne
Drop or pear	Bingera, Boogaldi, Charlotte, Puerta de Arauco, Uwet
Crescent shape	Avče, Bushman Land, Morradal
Oblate lenses (discoid)	Ballinoo, Colomera, Hill City, Kofa, Okano, Washington County
Prolate lenses (ovoid-cylindrical)	Babb's Mill (Blake), Föllinge, Juromenha, Lonaconing
Tongue shape	Nedagolla
Large, flat	Chupaderos, Campo del Cielo, Mbosi
Large, Ear shape	Bacubirito, Tucson (Carleton)
Thin, flat plates	Arlington, Bingera, Tawallah Valley
Elongated, prismatic	Guffey, New Leipzig, Osseo, Zacatecas (1792), Kopjes Vlei
Dumbbell shape	Savannah
Foot shape	Bald Eagle, Signal Mountain, Warburton Range
Octahedral, pyramidal	Lazarev, Novorybinskoe, Quesa, Rowton, Samelia, Sikhote-Alin, San Francisco Mountains
Hexahedral, cubic	Boguslavka, Calico Rock, Edmonton (Canada)
Angular, irregular	Bruno, Canyon Diablo, Cape York, Gibeon, Hoba, Juncal, Kayakent, Neptune Mountains, N Kandhla, Sikhote-Alin, Treysa, Youanmi
Same, Reentrant angles, irregular in the extreme	Bahjoi, Cruz del Aire, Edmonton (Ky.), Gibeon, Glorieta Mountain, Mesa Verde, Mungindi, Sikhote-Alin, Silver Crown, Tazewell, Thule, Thunda
Spikes, icicles	Glorieta Mountain, San Cristobal
Rings, imperfect rings	Hex River, Kokstad, Mount Magnet, Tucson (Ring)
Bombshells, twisted slugs, often slicken-sided	Canyon Diablo, Henbury, Imilac, Sikhote-Alin

Figure 31. The large, ear-shaped Bacubirito mass is presently exhibited in Culiacan, Mexico. It is 4.2 m long and may be estimated to weigh 22 ton. The white ruler measures 15 cm.

Figure 32. Morito, an eminent 10.1 ton cone-shaped meteorite, on display in Mexico City. Height of cone 105-110 cm. Width in two perpendicular directions 190 and 140 cm. Note the oriented regmaglypts.

glypts. Transitional stages are represented by pear-, tongue- and crescent-shaped masses.

Completely anomalous are the two thin plates of Tawallah Valley (76 kg, ~ 6 cm thick) and Arlington (9 kg, 2.5 cm thick). They are probably best understood as spallation products from a preatmospheric collision. The almost whole plates miraculously survived entry without bending or showing any signs of distortion, probably due to a low angle, coasting trajectory.

Regmaglypts

A specific hallmark of an iron meteorite are the regmaglypts. For some historical notes, see page 1002 and Berwerth (1909). Regmaglypts are thumb-like pits carved into the surfaces by turbulent supersonic airstreams during the atmospheric flight. Stones show them occasionally but not to the perfection seen in irons. Although they vary in shape and size, when well developed, they usually have a diameter about a tenth of the meteorite itself, measured in a direction perpendicular to its movement. The ratio of diameter to final mass is particularly well displayed on a selection of samples from large showers, such as Glorieta Mountain and Sikhote-Alin. No doubt the relative size and shapes of the regmaglypts must be of more than casual interest to the physicist or engineer who is engaged in the study of supersonic airflow. For example, when examining the shape of regmaglypts, one is left with the impression that the majority of iron meteorites for some reason travel in such a position that they encounter the resisting air broadside; i.e., in a maximum-drag orientation. Since, as mentioned above, the preatmospheric shape of the meteorites is apparently tabular or pyramidal, the drag coefficient

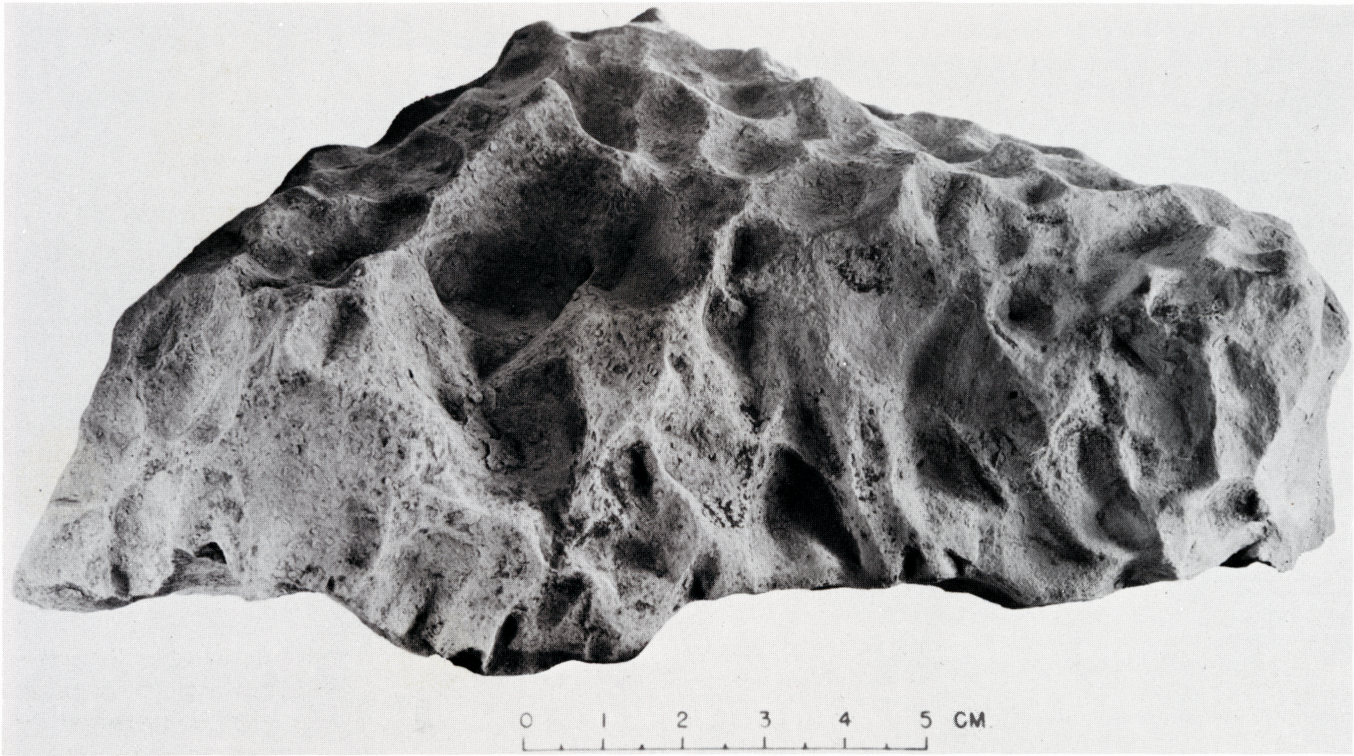

Figure 33. This 3.85 kg Henbury specimen (U.S.N.M. no. 1492) is a remarkably well-preserved shield-shaped sample, which is almost a true miniature of the much larger 181 kg sample on display in the Smithsonian Institution (No. 933). This type of material probably escaped the cratering impact and preserves the original structures. Compare Figure 34. Vapor-coated with NH_4Cl before photographing. S.I. neg. M-22c.

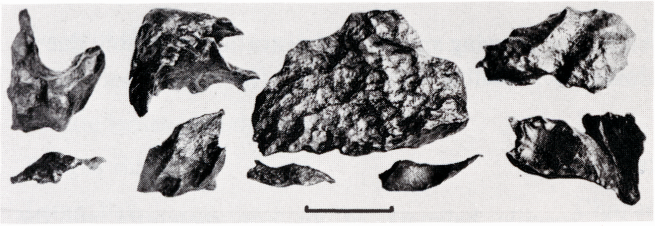

Figure 34. Henbury. A collection of the curiously torn fragments found in thousands around some of the craters. These samples are severely shocked and annealed. (From Hodge-Smith 1939.) Scale bar approximately 5 cm.

to be applied in equation 1, page 20, is rather 1.2-1.4, than the usually applied 0.8-1.0, which is based on the assumption of an initial spherical shape.

On meteorites that tumble through the atmosphere the regmaglypts are more or less equiaxial in shape and evenly distributed upon the different surfaces. On oriented meteorites the regmaglypts are elongated in the flight direction and thus may serve to indicate the apex or the "brustseite." It has often been stated that the regmaglypts are caused by the burning of low-melting minerals, such as troilite and schreibersite, but this is not the case. The regmaglypts are usually too densely spaced and too regularly arranged to

Figure 35. Glorieta Mountain (U.S.N.M. no. 905). The finger-shaped "icicle" which weighs 290 g was produced by fragmentation in the atmosphere. S.I. neg. 31801 -A. Scale bar 3 cm.

Figure 36. Boogaldi. A smooth pear-shaped mass of 2.05 kg. (From Hodge-Smith 1939.) Scale bar 5 cm.

have been caused by dubious postulated inclusions or low-melting phases. They are more likely the result of hot, turbulent supersonic airstreams along the body. Numerous iron meteorites with almost homogeneous structures thus display regmaglypts; e.g., Bacubirito, Gibeon, and Boguslavka.

It appears that the major part of the regmaglypts developed during the high velocity part of the trajectory, probably within a few seconds when the velocity was still above 10 km/sec. If such velocities are maintained down to the denser atmosphere below an altitude of 25-30 km, the regmaglypts apparently develop in profusion. This may be part of the explanation why regmaglypts are rare on stony meteorites: These have usually lost most of their cosmic velocity at somewhat higher altitudes.

Boguslavka is an interesting case. At high velocity, the primary surfaces of the entire hexahedrite became covered with deep and densely spaced regmaglypts. Then, late in flight, the 250 kg mass split along a hexahedral cleavage plane, and the fracture crossed a number of regmaglypts. The two fragments fit together well, and it can be seen how

Figure 37. Bushman Land (U.S.N.M. no. 2515). A well-preserved 3.0 kg mass with smoothly rounded parts and with a slightly concave side covered with regmaglypts. S.I. neg. 1532A. Scale bar 5 cm.

the initial regmaglypts are almost unaltered in the subsequent flight. However, the two fragments still had sufficient velocity for new regmaglypts to start to develop on the plane cleavage faces. These regmaglypts are shallow and broad, but otherwise resemble the mature regmaglypts on the primary surfaces.

On cone-shaped bodies, e.g., Morito, Quinn Canyon, Cabin Creek and Hraschina, there is a marked difference between the regmaglypts on the tapering sides and the rather flat rear side. The first mentioned are deeply carved, with elongated grooves radiating from the apex; the last mentioned are shallow and about twice as wide as the others. Apparently the ablational power of an airstream on the rear of an oriented meteorite corresponds to the low velocity region in the last part of the trajectory.

Many iron meteorites display confusing mixtures of regmaglypts and rather smooth surfaces, e.g., Bahjoi, Bushman Land, Durango, Hill City, Hassi-Jekna and Repeev Khutor. Even on very small, smooth meteorites, e.g. Avče, Joel's Iron and Puerta de Arauco, regmaglypt-like depressions may be identified. It appears that the smooth parts of the meteorites were the last to develop, at relatively low velocities between 3 and 10 km/sec. Below 3 km/sec probably very little ablation occurred. If this supposition is correct, the effectively smoothed surfaces developed on meteorites which, because of a low angle of entry (φ), had a relatively long coasting flight at velocities below 10 km/sec. On the other hand, fully regmaglypt-covered masses should have had rather steep entries with short trajectories in the low velocity region.

The Atmospheric Heating and Ablation as Revealed by Metallographic Examination

Cuts perpendicular to the surface of a freshly fallen iron meteorite disclose fusion crusts and heat-affected rim zones. While the fusion crusts on stone meteorites are

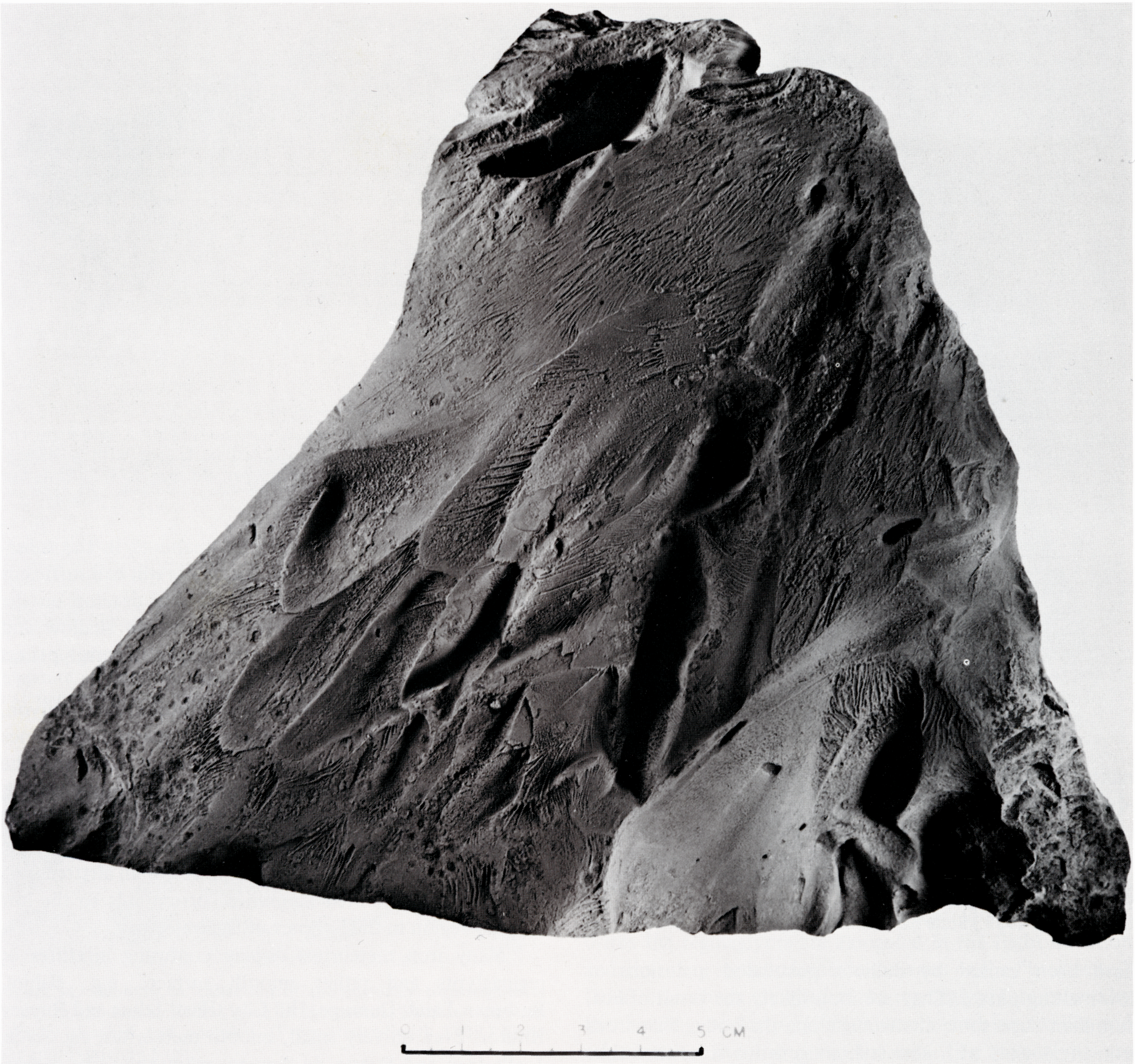

Figure 38. Bruno. An angular mass of 12.7 kg with five major faces and a sixth smaller one, all of which have been sculptured by ablation in the atmosphere. Elongated regmaglypts radiate from what was apparently the apex during flight. Fine hair-lines of metallic fusion crust are clearly seen. NH_4Cl-coated. Scale bar 5 cm.

usually the product of simple melting, the crusts on iron meteorites are complex, displaying mixed melts of fully and partially oxidized metal. The fusion crusts are the adhering remnants of ablated metal from the last part of the trajectory left on the surface when the velocity decreased below about 3 km/sec, and ablation ceased. In addition, some fusion and light-emission may have been caused by exothermal oxidation of iron in the denser parts of the atmosphere. The fusion crusts are, in principle, composed of an exterior fully oxidized, rapidly solidified nonmetallic melt, and an interior only slightly oxidized metallic melt. The oxide melts have solidified and decomposed to wüstite-magnetite aggregates, while the metallic melts, often forming numerous crossbedded 50 μ thin sheets, have solidified to dendritic-cellular aggregates, that below 700° C have transformed diffusionless to fine-grained martensitic α_2 products. They are usually hard, HV 310±50, but the hardness is of little informational value since it is widely scattered because of the numerous micropores and oxide inclusions. Also, the hardness measurements require perfect, edge-supported samples.

Figure 45 is a sketch of a typical ablated surface as it may be observed on, e.g., Bahjoi, Bogou, Juromenha and Yardymly. The interface between the fused layers and the

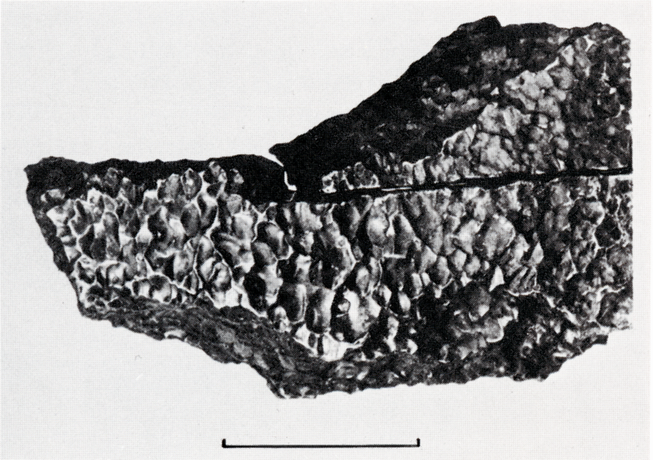

Figure 39. The Boguslavka hexahedrite. The second largest iron seen to fall. The mass split along a cubic cleavage plane and produced two fragments of 198 and 58 kg, here restored to original shape. Scale bar 20 cm. (Courtesy E.L. Krinov.)

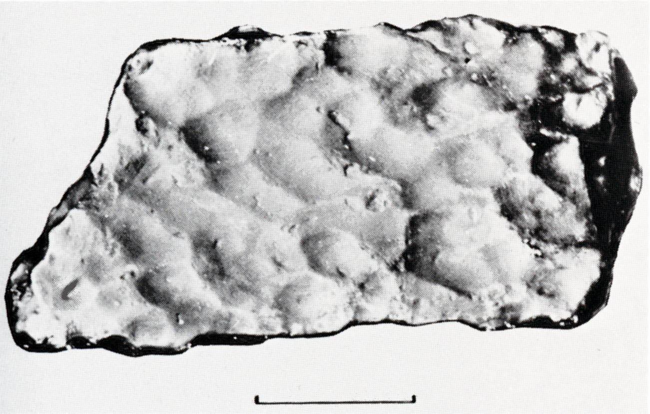

Figure 40. Boguslavka. The cleavage plane on the 58 kg mass. The flight was evidently sufficiently long for new shallow regmaglypts to be produced after splitting. Scale bar 10 cm.

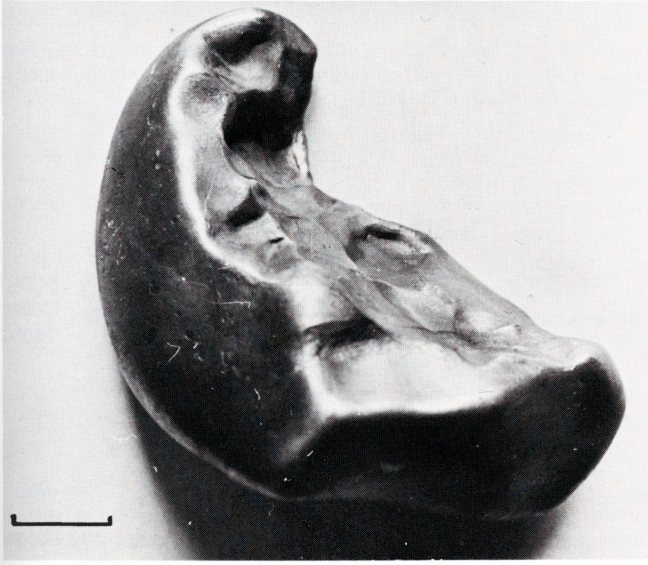

Figure 41. Avče. An eminent, softly rounded crescent of 1.23 kg with regmaglypts on the concave side. Scale bar 2 cm.

Figure 42. The stone meteorite Pasamonte (eucrite), New Mexico, fell as a shower March 24, 1933. The small individual shown here is entirely enveloped in a porous glass crust with numerous gasholes. This appearance is unknown in iron meteorites. NH_4Cl-coated. Scale bar 2 cm. S.I. neg. 19755.

unmelted meteorite is smooth on the large scale but irregular in details because it accurately reflects the melting temperatures of the phases present along the surface. Kamacite, with a melting point of about 1500° C, occupies the highest level. Taenite, which contains 30-40% Ni in solid solution and consequently has a 30-40° C lower melting point, is slightly excavated, leaving grooves 10-30 μ deep. Schreibersite with a melting point of 1000±10° C is severely attacked to depths of about 1 mm below the kamacite surface. The major part of the melted schreibersite is removed and only partly replaced by other metallic melts from adjacent sites. Grooves caused in this way and resembling chisel scars are often seen on ablated surfaces as a result of the burning out of Brezina lamellae (See, e.g., Grant, Chupaderos, Hammond and Kouga Mountains).

If pure, the troilite has a melting point about 1190° C. It will usually be excavated, as shown, leaving cylindrical cavities with flat bottoms. Only insignificant parts of the melts remain in the cavities. The troilite immediately below the melted surface will usually be recrystallized. Troilite, with significant inclusions of graphite and silicates, will be quite refractory and will ablate away at a rate comparable to that of the metallic surface. Some meteorites which are anomalously rich in troilite, such as Pitts and Soroti, will show anomalous ablation sculptures and anomalous fusion crusts.

Below the fusion crusts, a heat-affected zone follows. The examination of this zone is important because it (i) yields information of the flight characteristics and

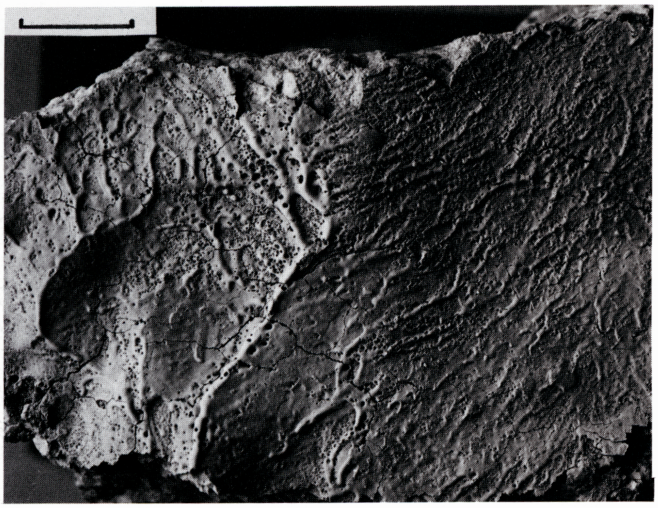

Figure 43. The stone meteorite Norton County (aubrite), Kansas, fell February 18, 1948. Close-up of warts, hair-lines and gasholes in the glassy fusion crust. Note also the numerous fine fissures. Scale bar 1 cm. S.I. neg. M-1360A.

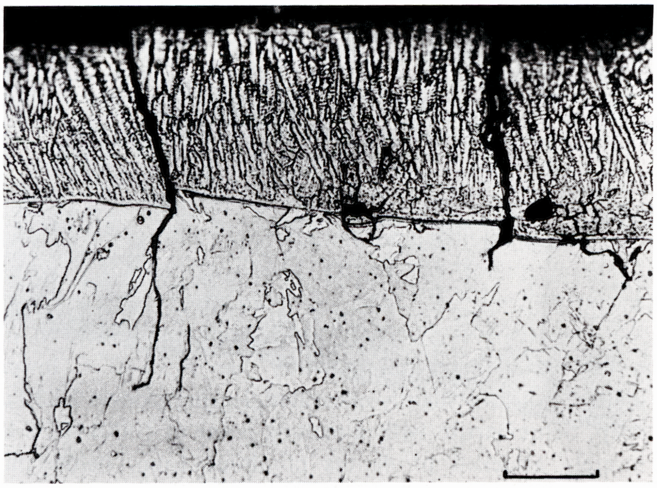

Figure 44. Mazapil (Chicago no. 1977) Above, the 100 μ thick dendritic-columnar metallic fusion crust. Below, the exterior part of the heat-affected α_2 zone. Note the fissures and the relative displacements in the metal, which cause the fusion crust to crack. Scale bar 40 μ.

Figure 46. Samelia (Brit. Mus. 1927, 916). To the left a part of the oxidic and metallic fusion crust. The taenite has a lower melting range than kamacite and is preferentially ablated. The kamacite is transformed to α_2, but near taenite it is modified to bainitic structures due to carbon. Etched. Scale bar 40 μ.

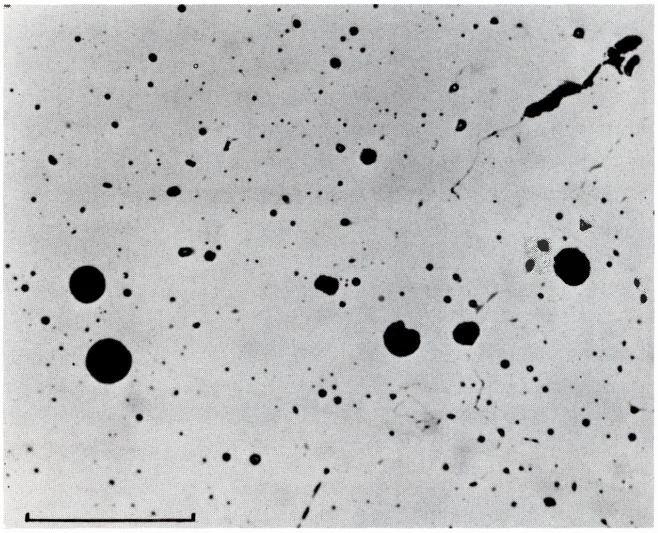

Figure 47. Mazapil (Chicago no. 1977). The metallic fusion crust contains numerous spherical gasholes and globular iron oxide melts. Polished, unetched. Scale bar 20 μ.

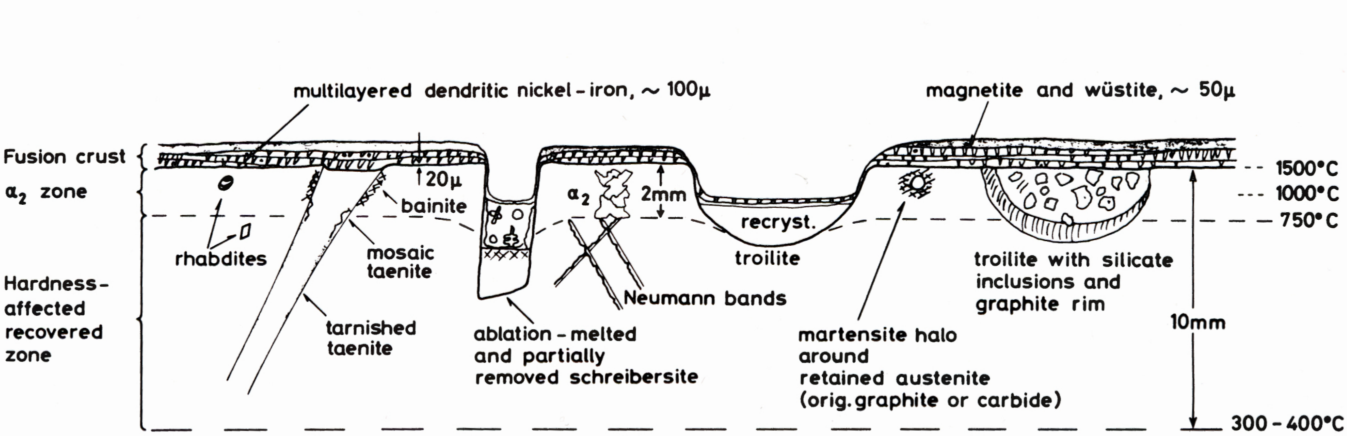

Figure 45. Sketch of the ablated surface of a typical iron meteorite. Below 2 mm, structural alterations are usually absent, and below 10 mm the microhardness is also unaffected. Not drawn to scale in details.

indicates the exact dimensions of the meteorite after the completed flight, even if some corrosion has occurred afterwards; (ii) allows qualitative estimates of the terrestrial age of the meteorite; (iii) displays in itself a remarkable constancy from meteorite to meteorite, so that it may be used as a reference zone; and (iv) indicates that artificial reheating has not occurred.

The typical heat-affected zone, as revealed by microhardness testing and etching, is 10 mm wide under a plane or slightly convex meteorite surface, Figure 45. Under concave surfaces, for example, at the bottom of regmaglypts, the zone decreases to below 4 mm, while under knobs and strongly convex surfaces the zone increases to thicknesses of 20 or even 30 mm. The normal 10 mm wide zone may be divided into three easily recognizable subzones.

A. The outermost 1 mm will display micromelted phosphides, corresponding to brief peak temperatures above 1000° C. Originally angular, the phosphides have now assumed subspherical shapes since, upon melting, they have dissolved part of the adjacent metallic walls. Fine, zigzagging, 1-2 μ wide veinlets of phosphide melts follow the high temperature austenite grain boundaries and have often caused fissures perpendicular to the surface, resembling hot-cracking in cast steels. The phosphide melts have solidified by cooling from the massive interior, as clearly evidenced by the direction and location of the primary dendrites. The remaining melts have solidified in extremely fine-grained eutectic structures. Spherical gasholes, 5-25 μ across, have very often developed during the solidification. These pinholes are characteristic for the exterior zone.

B. The outermost 2 mm, and thus comprising zone A, is the heat-affected zone familiar to most people. When etching a good polished section, it develops distinctly as a matte rim, following the contours of the meteorite. It is

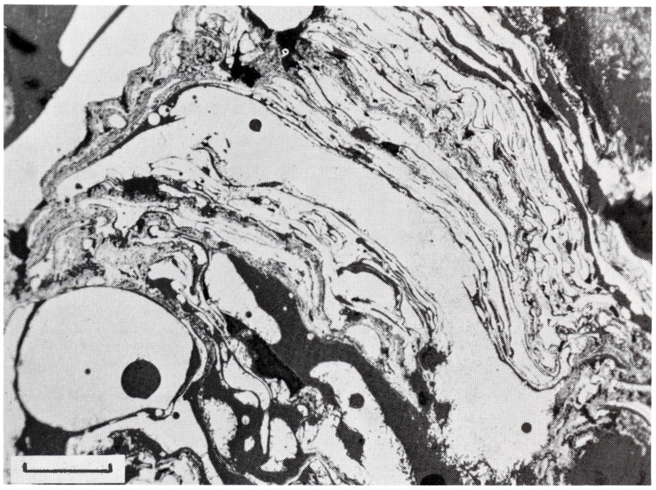

Figure 48. Kalkaska (U.S.N.M. no. 3217). On certain parts of the ablated surface, intricate whirlpools of fused metal and fused iron oxides are deposited. Polished, unetched. Scale bar 30 μ.

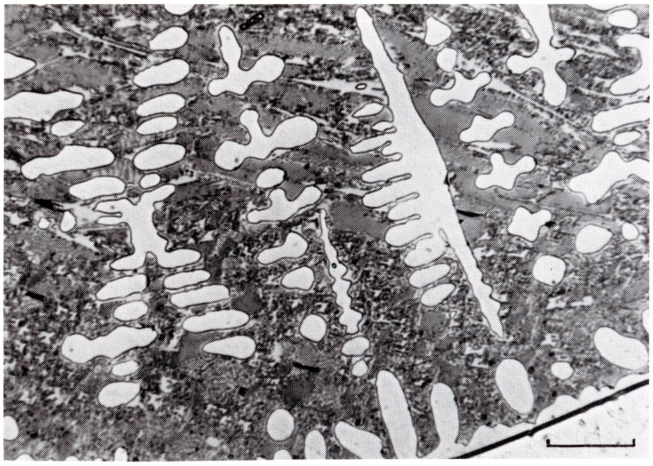

Figure 50. Silver Crown (U.S.N.M. no. 522). A completely molten and rapidly solidified schreibersite particle. The primary dendrites are dispersed through the melt and line the smooth wall. The melt finally solidified to an extremely fine-grained eutectic at about 1000° C. Etched. Scale bar 25 μ.

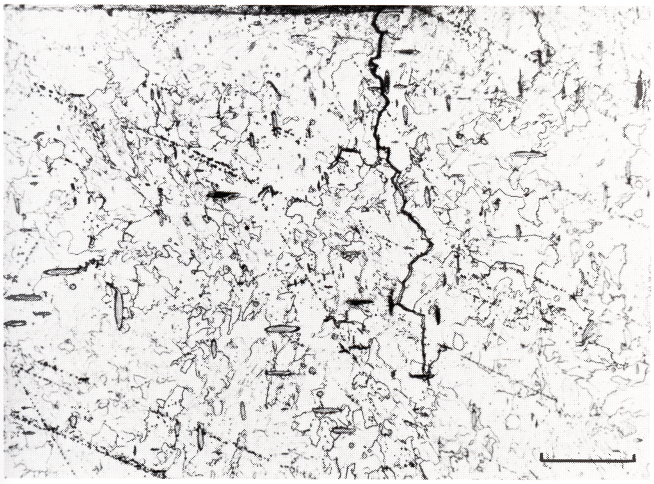

Figure 49. Yardymly (U.S.N.M. no. 1940). Fusion crust above. Heat-affected zone A with α_2 transformation structure, micromelted phosphides and surviving precipitates on the former Neumann bands. A microfissure filled with phosphide melt extends perpendicular to the surface through zone A. Etched. Scale bar 200 μ.

Figure 51. Washington County (Harvard no. 565). On this anomalous meteorite the heat-affected zone A has acquired a peculiar matte sheen due to a large number of microscopic pinholes. The shrinkage cavities (black on the photo) are located in the last solidifying phosphide eutectics, nearest the ablated surface. Etched. Scale bar 50 μ.

caused by the rapid, diffusionless transformation of kamacite to unequilibrated serrated α_2 structures: $\alpha \rightarrow \gamma \rightarrow \alpha_2$, a reaction which occurs when the temperature briefly exceeds 750° C. The α_2 grain size is small (5-25 μ) when produced from a shock-hardened hatched structure but large (50-200 μ) when produced from an annealed structure or from a structure with Neumann bands. The hardness is almost the same, HV 190±30, whatever the initial kamacite structure. More important to the resultant hardness and to the structural details is the amount of phosphorus and nickel in the meteorite. Increasing amounts of these elements tend to increase the α_2 hardness to about 250 by solid solution hardening.

If carbon is also present, martensitic-bainitic zones, with hardnesses in excess of 350, may form. Such products are very common in 20-100 μ wide zones adjacent to taenite with carbon in solid solution. The taenite which usually stains in brown-blue colors in the interior of the meteorite – possibly due to a submicroscopic decomposition to $\alpha + \gamma$ – reacts differently in the rim zone. It etches in clear whitish colors, apparently because the $\alpha + \gamma$ mixture has homogenized to pure γ. Simultaneously, the taenite has recrystallized to polycrystalline aggregates of 50-100 μ grains, each of which has imperfectly transformed to martensitic α_2 structures upon cooling. The resultant α_2 structures vary in appearance with the actual nickel content. Taenite with more than about 30% Ni will not transform to α_2 as shown by Allen & Earley (1950) and Kaufman & Cohen (1956), and, therefore, remains more or less structureless, Figure 181. Its hardness is, however, usually significantly altered.

While the α_2 zone is usually 2.0±0.5 mm wide under the leading surface in stabilized flight, it may increase to 4±1 mm on the rear surfaces, see e.g., Costilla Peak, Keen Mountain, Serrania de Varas and Washington County. Under unusual flight circumstances the α_2 zone may even increase to 6 or 8 mm width, such as recorded in Chupaderos and Roebourne. On the other hand, on fracture surfaces which were produced late in flight, the α_2 zone may be very thin, for example 0.8±0.4 mm on specimens of Soroti, Toluca, Imilac and others.

C. The innermost 8 mm of the heat-affected zone usually escapes notice. It is hardly to be seen by normal optical microscopy but is readily revealed by microhardness testing. Hardness tracks, preferably applying 50-100 g

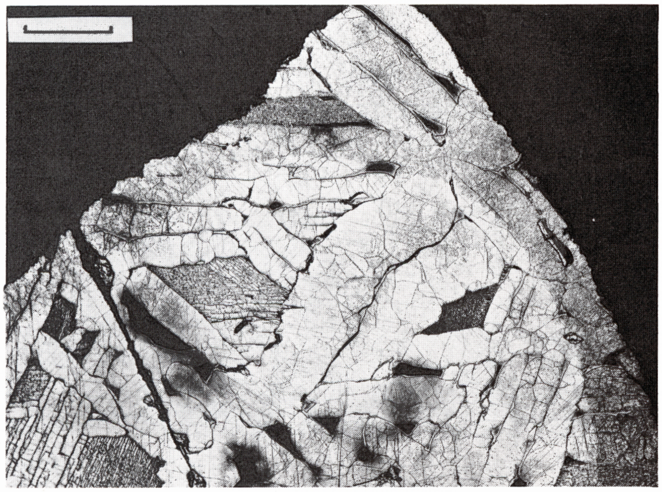

Figure 52. Thule (Copenhagen no. 1955, 186). The heat-affected rim zone B is seen as a smoothly curved, matte exterior zone. Its matte appearance is due to kamacite having transformed to unequilibrated α_2 whenever the temperature briefly exceeded 750° C. Etched. Scale bar 3 mm.

Figure 53. Mazapil (Chicago no. 1977). A detail of the heat-affected B zone of 800-1000° C. Transformation of α_2 into kamacite, and mosaic pattern – actually in yellow to brown hues – within the taenite. Etched. Scale bar 100 μ.

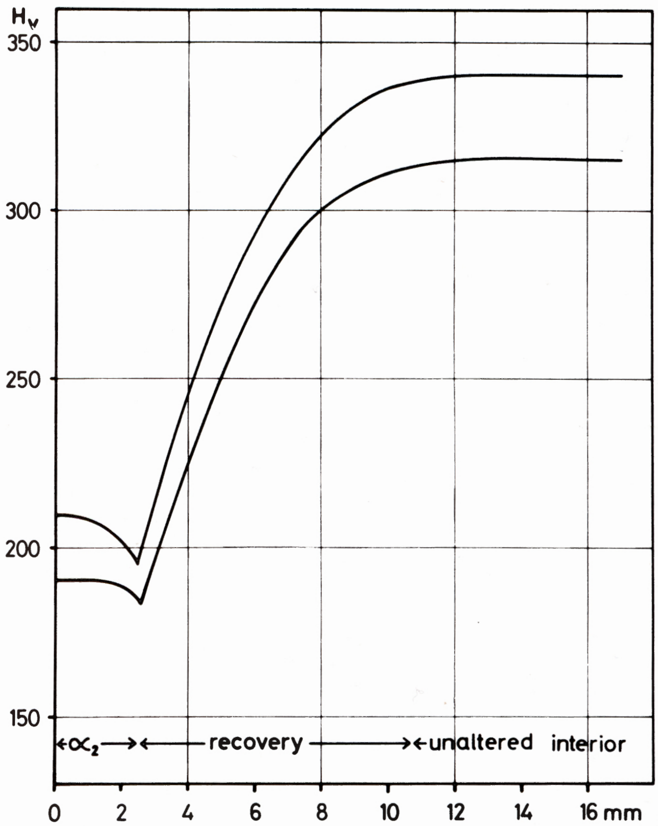

Figure 54. Hardness curve type I. Hardness (100 g Vickers) versus depth below the ablated surface of an iron meteorite. Since hardness measurements scatter significantly, the hardness results are shown as a *band* within which 90% of all measurements are situated.

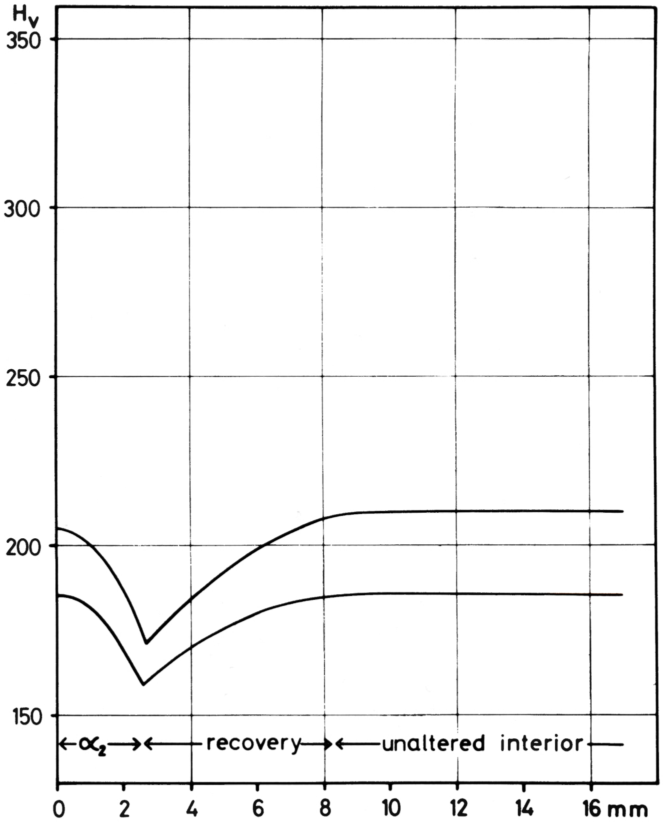

Figure 55. Hardness curve type II.

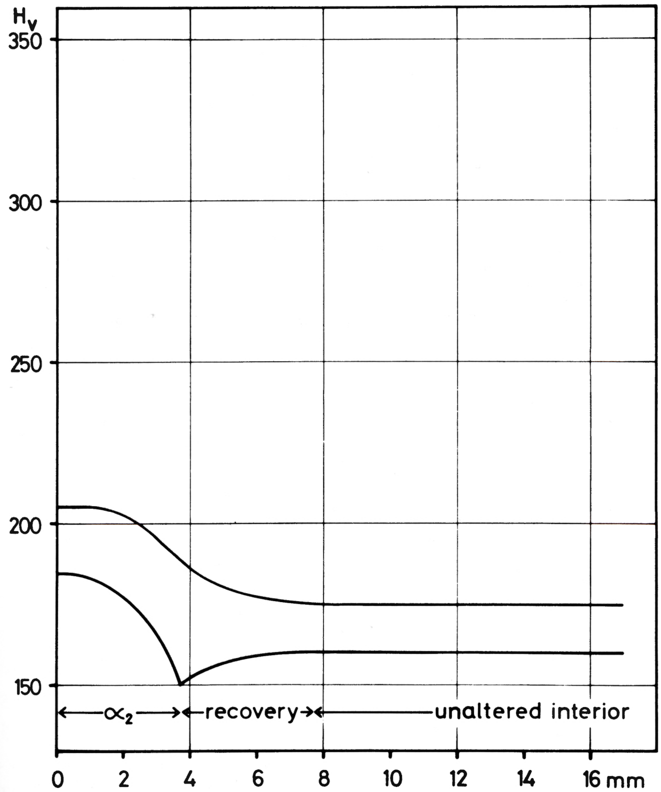

Figure 56. Hardness curve type III.

loads on a Vickers Pyramid indenter, indicate significant hardness variations, as shown in Figures 54-59. Common to

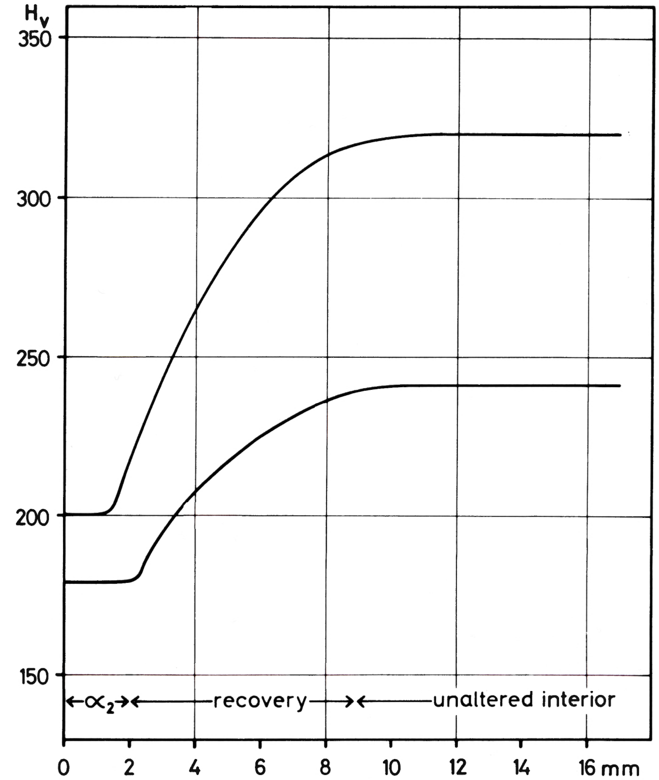

Figure 57. Hardness curve type IV.

these curves is the hardness level of the α_2 zone, 200±20. Below this zone – i.e., below peak temperatures of 700-750° C – the α_2 transformation cannot occur. Instead, the kamacite is recovered; there was usually insufficient time for recrystallization, and the term "recrystallized rim zone" for any of the zones A, B or C is very inadequate although it has been used by many authors in the past in rather inaccurate descriptions.

Curve I illustrates the case when the meteorite, because of cosmic shock events, has acquired a high initial hardness, the kamacite easily reaching 300-350. During the brief atmospheric reheating, the kamacite recovers and hardnesses reach minimum values of 180 just below the zone which has transformed to α_2. Excellent examples are found in Bartlett, Drum Mountains, Grant, Kalkaska, Savannah and View Hill.

Curve II illustrates the case when the original hardness was medium due to low shock intensities or to imperfect cosmic annealing of highly shocked material. The atmospheric annealing serves to decrease the hardness further to about 170 in the recovered transition zone. Examples are to be found in Bogou, Bushman Land, El Burro, Perryville, Seymour and Wabar.

Curve III illustrates the case when the meteorite was in an almost perfectly annealed state before it reached the Earth's atmosphere. Little extra recovery is to be expected in such a case. Examples are to be found in Ballinoo, Edmonton (Canada), Indian Valley, Joel's Iron and Yardymly.

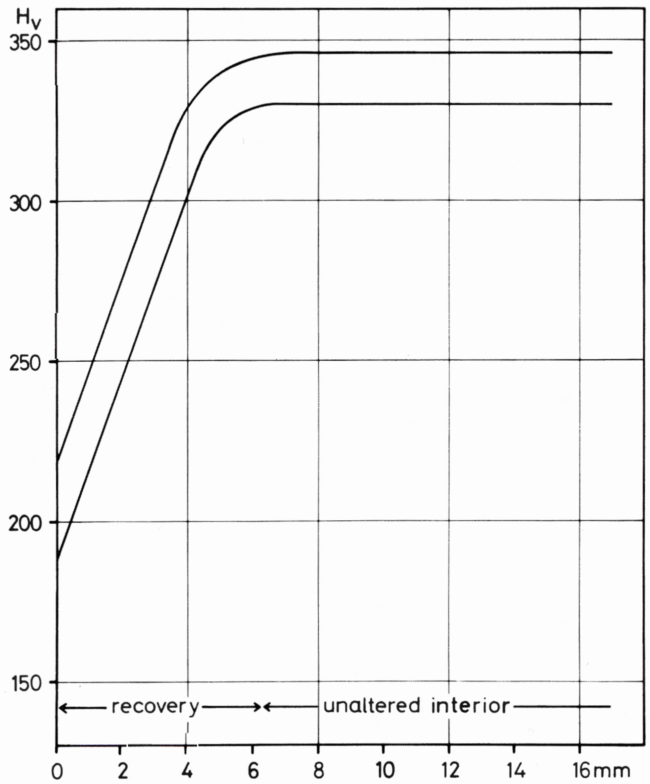

Figure 58. Hardness curve type V.

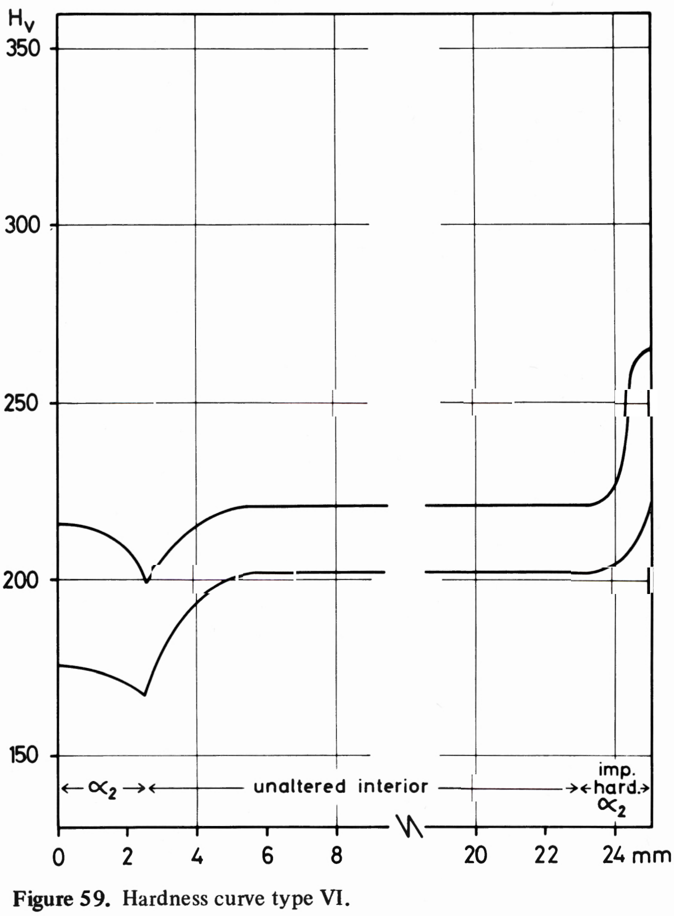

Figure 59. Hardness curve type VI.

Curve IV illustrates the rather few cases where the meteorite displays a wide range of hardnesses, either because of preatmospheric inhomogeneous cold work or because of atmospheric breakup and cratering effects. Within a few square centimeters of a section the hardness may vary 100 units, but in the α_2 zone the hardness is, as usual, about 200; all effects of previous inhomogeneous cold work have disappeared. Examples are to be found in Cape York, Gibeon, Madoc, Osseo, Russel Gulch and Wood's Mountain.

Curve V illustrates the case where kamacite is too sparse for a hardness track to be obtained within this phase. Instead, the taenite phase has been measured, e.g., in the ataxites Freda, Illinois Gulch and Twin City. The taenite exhibits a smoothly decreasing hardness towards the surface. This is because the taenite – with 35-45% Ni – at all temperatures lies in a stable austenite part of the Fe-Ni diagram, with no possibilities of $\alpha \rightleftarrows \gamma$ transformation. The curve also illustrates the hardness of 40-60 μ wide taenite (35-45% Ni) lamellae of typical octahedrites, e.g., Bagdad, Cape York, Grant, Kayakent, N'Kandhla and Neptune Mountains. However, the taenite lamellae, which are somewhat inadequate for routine hardness tracks because they only cover a small percentage of the whole section, may be insufficiently represented in the heat-affected zones for a full hardness track and may alter their chemical composition in the most heated near-surface regions, thus impairing the hardness comparisons.

Curve V compared to curves I-IV indicates that cold-worked taenite is slower to recover than the adjacent kamacite and that taenite does not usually, during the brief atmospheric flight, acquire the minimum values, 155, which are obtained by more thorough annealing.

Finally, curve VI illustrates an unusual case, so far only observed once, in Jamestown, but probably also occurring in other irons with a similar flight history. The curve illustrates a hardness track across a 25 mm thick section of Jamestown, page 690. The left ablation surface displays a normal type II hardness curve, while the entire middle portion represents the cosmic, initial hardness. However, the opposite ablation surface displays hardening effects of an unusual character. Microscopic examination reveals the cause of the high hardness. Numerous fine metallic and oxidic spherulites have apparently impacted the metallic surface late in the flight and have been partly cold-welded to the surface. In several places the linear elements of the Widmanstätten structure are severely bent and distorted around the impacting particles. It is worth noting here that Jamestown is of airfoil shape. Relatively slow ablation occurred on the convex side, while the flat or concave opposite side was rapidly devoured and in the later stages impact-hardened, presumably due to fused particles carried in the intensive eddies of the passing air.

Figure 61 summarizes the results for kamacite and taenite lamellae in a typical octahedrite. The associated peak temperatures are estimated from laboratory experiments in which synthetic Fe-Ni-P alloys and selected iron

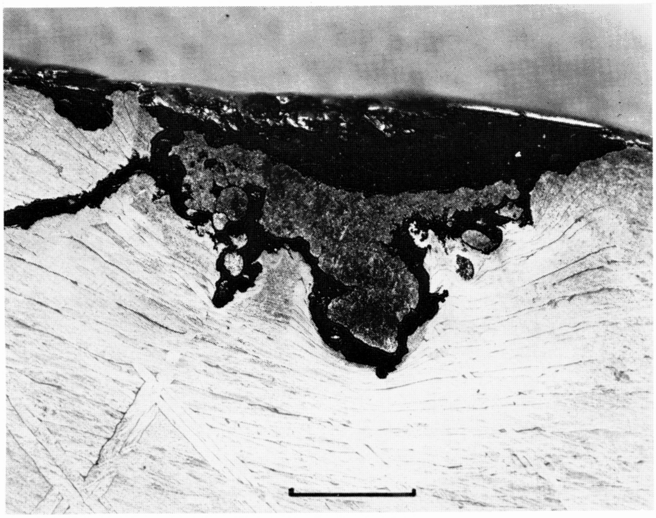

Figure 60. Seneca Township (U.S.N.M. no. 1325). Section perpendicular to the surface. Whirlpool structure of the ablated and redeposited fused metal. Severe plastic deformation of the underlying Widmanstätten structure. (Perry 1950: volume 4.) Scale bar 1 mm.

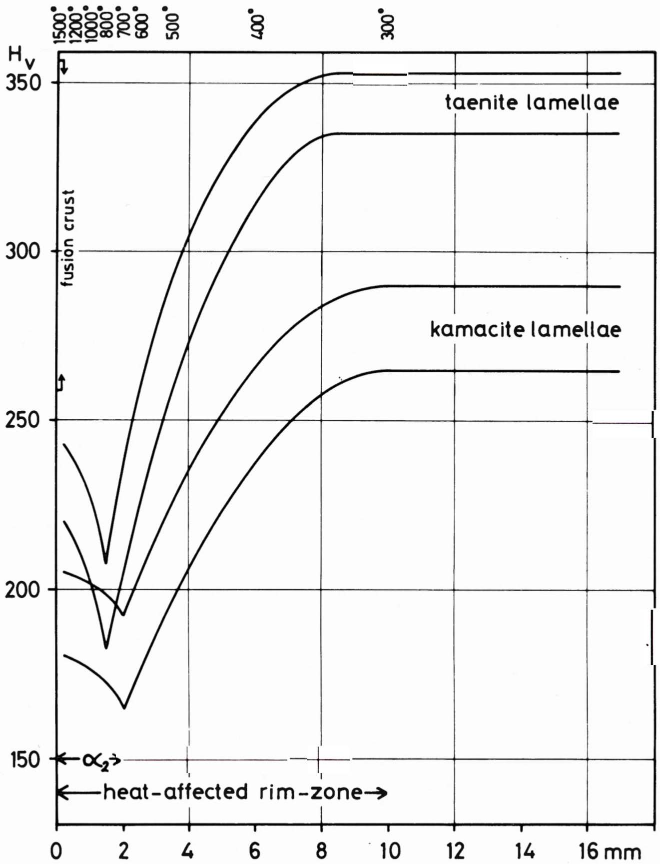

Figure 61. Hardness curves for typical kamacite and taenite lamellae of the same iron meteorite, such as Thule or Grant. The heat-affected zone is 10 mm deep, but optically visible changes are only present in the exterior 2 mm.

meteorites were subjected to brief reheatings to the temperatures indicated. No effects were found below 300° C. The hardness of taenite in the outermost 1 mm is not well determined, but the trend is clear. It appears that the hardness, much higher than expected from curve V, is due to diffusion reactions so that the taenite lamellae in this high temperature region have lower nickel contents (18-25%) than in the interior (35-45%) and, therefore, acquire higher hardnesses upon quenching (see, e.g., Buchwald 1966, Figure 13).

The importance of the hardness curves I-VI lies in their support and extension of the observations which are possible with the microscope. With the aid of these curves, the position of the meteorite's surface may be extrapolated with precision, even if later corrosion has removed the visible α_2 part of the heat-affected zone. Weathered meteorites, e.g., Boxhole, Cleveland and Davis Mountains, may thus exhibit only the right leg of curve I, but the results discussed here allow us to estimate the loss in millimeters. In addition, if we know the climatic conditions of the place of find and the depth of burial, we may eventually hope to reach a semiquantitative terrestrial age, i.e., the number of years the meteorite has been exposed to terrestrial weathering.

Another very important aspect of the heat-affected zones lies in the fact that we may now definitely deduce the size of the body in the last part of the trajectory. No wild speculations regarding the amount of silicate material once present as a wrapping – but now supposedly weathered away – can be allowed. When the criteria developed above are fulfilled for the heat-affected zone, we know exactly how much larger the meteorite could have been immediately after its fall. This aspect is important because a large proportion of all iron meteorites, about 94%, are usually finds of an undetermined age.